Hybrid TiO$_2$–SnO$_2$ Nanotube Arrays for Dye-Sensitized Solar Cells

Umang V. Desai, Chengkun Xu, Jiamin Wu, and Di Gao*

Department of Chemical and Petroleum Engineering, University of Pittsburgh, Pittsburgh, Pennsylvania 15261, United States

S *Supporting Information*

ABSTRACT: Tin oxide (SnO$_2$) is a promising wide band gap semiconductor material for dye-sensitized solar cells (DSCs) because of its high bulk electron mobility. Employing vertically ordered 1-D nanostructures of SnO$_2$ as the photoanode may overcome the limit of current DSCs by using new redox mediators with faster kinetics than currently used ones. Synthesizing such nanostructures and integrating them into DSCs, however, has been proven challenging. Here, we demonstrate that, by using ZnO nanowires as a sacrificial template, vertically aligned SnO$_2$ nanotube arrays may be feasibly synthesized through a liquid-phase conversion process, and the synthesized SnO$_2$ nanotubes can be further coated with a thin layer of TiO$_2$ to form hybrid TiO$_2$–SnO$_2$ nanotube arrays.

Both the resulting SnO$_2$ and hybrid TiO$_2$–SnO$_2$ nanotube arrays are used to fabricate DSCs, and the best performing cell delivers a promising efficiency of 3.53%. Transient photovoltage measurements indicate that the electron recombination lifetime in hybrid TiO$_2$–SnO$_2$ nanotubes is significantly larger than those in TiO$_2$ nanotubes, ZnO nanowires, and films of sintered TiO$_2$ nanoparticles, suggesting promise of the TiO$_2$-coated SnO$_2$ nanotubes for further improvement of DSCs.
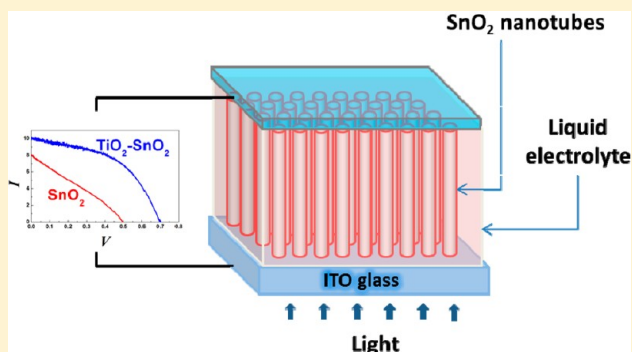
■ INTRODUCTION

Dye-sensitized solar cells (DSCs) based on metal oxide semiconductor photoanodes have attracted considerable interest for solar energy harvesting and conversion.[1,2] Efficiencies of up to 12% have been reported by using a mesoporous film of sintered TiO$_2$ nanoparticles as the photoanode.[3] The main advantage of using a random nanoparticle network is the high surface area available for dye adsorption, leading to improved light harvesting. However, further improvements in device performance have been limited by the poor electron transport characteristics of TiO$_2$ nanoparticle films.[4] In addition to TiO$_2$, various metal oxide semiconductors, including ZnO,[5] SnO$_2$,[6] and Nb$_2$O$_5$,[7] have been studied for their potential use as photoanodes in DSCs. Among these, SnO$_2$ is one of the most promising wide band gap semiconductor materials for DSCs. Bulk electron mobility in SnO$_2$ (μ_e = 100−200 cm^2 V^{-1} s^{-1})[8] is orders of magnitude higher than TiO$_2$ (μ_e < 1 cm^2 V^{-1} s^{-1})[4] and comparable to ZnO nanowires (μ_e = 200 cm^2 V^{-1} s^{-1}).[9] The high electron mobility may open up possibilities to further improve DSCs, for example, by using redox mediators with faster kinetics than currently used ones.[10,11] Very fast electron injection into SnO$_2$ from the excited dye molecules has also been reported ($\approx$150 ps) which is comparable to TiO$_2$.[12] Furthermore, use of SnO$_2$ as a photoanode may make the DSC less susceptible to UV degradation, due to the large band gap of SnO$_2$, leading to better long-term stability than DSCs employing ZnO or TiO$_2$ electrodes.[13,14]

Mesoporous films of SnO$_2$ nanoparticles have been used as photoanodes in DSCs.[6,7] The efficiencies of these DSCs, however, have been less than those using TiO$_2$ nanoparticles. The open-circuit voltage (V_{OC}) of SnO$_2$ nanoparticle-based DSCs has been limited to less than 0.4 V.[6,7,15,16] Such a small V_{OC} prohibits further exploration of using mesoporous films of SnO$_2$ nanoparticles as photoanodes for DSCs. As a promising alternative to sintered nanoparticles, 1-D nanostructures facilitate electron transport by providing a direct conduction pathway for the electrons. Gubbala et al. have used SnO$_2$ nanowires as photoanodes in DSCs, and a V_{OC} of 0.56 V is obtained, a 0.2 V increase compared to DSCs that use sintered SnO$_2$ nanoparticles.[15] Although a V_{OC} of 0.56 V is still too low to be considered for DSC applications, this result indicates that 1-D nanostructures may overcome some of the limitations of sintered nanoparticles. The SnO$_2$ nanowires in their DSCs, however, are randomly placed on the substrate, and therefore, the advantages of 1-D nanostructures may not be fully taken. In DSCs, photogenerated electrons need to travel through the sensitized film to be collected before they recombine. Apparently, aligning the 1-D nanostructures vertically across the thickness of the sensitized film, compared to random placement, provides a significantly more efficient path for electron transport and thus can reduce the recombination probability of photogenerated electrons. In addition, vertically aligned 1-D nanostructures also provide straight channels for filling the sensitized film with solid-state electrolytes, which is a promising approach to solve the packaging challenge and
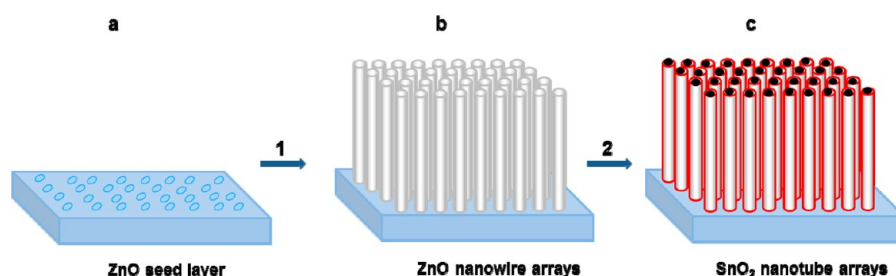
Figure 1. Schematic of the process for synthesizing vertically aligned SnO$_2$ nanotube arrays.

improve the long-term stability of DSCs. Therefore, vertically aligned 1-D nanostructures have recently attracted considerable interest for their potential use as photoanodes in DSCs. Both vertically aligned ZnO nanowires[5,17] and TiO$_2$ nanotubes[18] have been used to fabricate DSCs, and indeed, faster electron transport and improved electron collection efficiency, compared to photoanodes based on sintered nanoparticles, has been reported. DSCs fabricated by using vertically aligned SnO$_2$ 1-D nanostructures, however, have not been reported, primarily due to the difficulty in synthesis of such nanostructures.

Here, we report a method for synthesizing vertically aligned SnO$_2$ nanotube arrays by using ZnO nanowire arrays as a sacrificial template. The sacrificial ZnO nanowires are converted to SnO$_2$ nanotubes via liquid-phase SnO$_2$ deposition and simultaneous ZnO dissolution. The resulting SnO$_2$ nanotube arrays are used to fabricate DSCs, showing improved photovoltaic performance compared to SnO$_2$ nanoparticle-based devices. In addition, it is found that coating the SnO$_2$ nanotubes with a conformal thin layer of TiO$_2$ leads to a significant increase in open circuit voltage (V_{OC}) and fill factors (ff) for the DSCs, resulting in much higher efficiencies. Transient photovoltage measurements indicate that the photogenerated electron lifetime in the hybrid TiO$_2$–SnO$_2$ nanotubes is substantially longer than that in TiO$_2$ nanoparticles, TiO$_2$ nanotubes, and ZnO nanowires, suggesting promises of the TiO$_2$-coated SnO$_2$ nanotubes for further improvement of DSCs.

■ EXPERIMENTAL SECTION

**Synthesis of Arrays of ZnO Nanowires, SnO$_2$ Nanotubes, and Hybrid TiO$_2$–SnO$_2$ Nanotubes.** ZnO nanowire arrays were grown directly on indium doped tin oxide (ITO)-coated glass substrates. The substrates were first cleaned by acetone/ethanol sonication and rinsed thoroughly with deionized (DI) water. The substrates were then subjected to ultraviolet ozone (UVO) to remove any residual organics. The clean substrates were seeded by spin coating with 5 mM zinc acetate solution in ethanol followed by thermal decomposition at 300 °C. The seeded substrates were placed in an aqueous growth solution containing 0.025 M zinc nitrate, 0.0125 M hexamethylenetetraamine, 0.005 M polyethylenimine, and 0.35 M ammonium hydroxide at 90 °C for 6 h. The synthesized ZnO nanowire arrays were then rinsed with DI water and calcined in air at 450 °C for 1 h. For SnO$_2$ conversion, 0.15 M bulk solution of ammonium hexafluorostannate (AHFS) ((NH$_4$)$_2$SnF$_6$) (Aldrich) was prepared by dissolving 4 g of AHFS in 100 mL of water. The aqueous solution for conversion was prepared by mixing 3 mL of 0.15 M AHFS, 1 mL of 0.5 M H$_3$BO$_3$, and 1 mL of water. The nanowire array was then placed in this aqueous solution of 0.09 M ((NH$_4$)$_2$SnF$_6$) and 0.1 M H$_3$BO$_3$ at room temperature for 30 min, which resulted in the

formation of a vertical SnO$_2$ nanotube array. The synthesized SnO$_2$ nanotube array was then calcined in air at 450 °C for 1 h. For synthesizing hybrid TiO$_2$–SnO$_2$ nanotube arrays, a thin layer of TiO$_2$ was deposited on the surface of SnO$_2$ nanotubes by immersing the SnO$_2$ nanotube array in a solution of 0.1 M (NH$_4$)$_2$TiF$_6$ and 0.2 M H$_3$BO$_3$ for 20 min. This solution was prepared by mixing 3 mL of 0.1667 M bulk solution of ammonium hexafluorotitanate (AHFT) ((NH$_4$)$_2$TiF$_6$, Aldrich), prepared by dissolving 3.3 g of AHFT in 100 mL of water and 2 mL of 0.5 M H$_3$BO$_3$. The TiO$_2$ nanoparticle-based electrode was prepared by applying a paste of TiO$_2$ nanoparticle onto the conducting substrate (ITO) by doctor blading. The paste used consisted of commercially procured TiO$_2$ nanoparticles (15 nm) dissolved in 10 mL of ethanol and 0.2 mL of isopropoxide. The TiO$_2$ nanoparticle film obtained by this method was 10–11 μm thick. The method used for synthesizing TiO$_2$ nanotubes has been published by our group before.[18]

Fabrication and Characterization of DSCs. The synthesized nanotube arrays were immersed in 0.5 mM (Bu$_4$N)$_2$[Ru(4,4′-(COOH)-2,2,-bipyridene)$_2$(NCS)$_2$] (N719 dye) in ethanol overnight. A 60 μm thick hot melt sealing film (SX 1162-60, Solaronix) was sandwiched between the nanotube array and the platinized counter-electrode. A solution containing 0.1 M LiI, 0.1 M I$_2$, 0.5 M *tert*-butylpyridene, and 0.6 M tetrabutylammonium iodide in acetonitrile was used as the electrolyte. Cells were tested under AM 1.5G simulated sunlight (model 67005, Oriel) using a Reference 600 Potentiostat (Gamry Instruments). Photovoltage decay experiments and electrochemical impedance spectroscopy (EIS) were carried out using the same Reference 600 Potentiostat. EIS spectra were measured at open-circuit voltage under illumination of 100 mW/cm^2 AM 1.5G simulated sunlight and under dark conditions. The frequency range is 0.01–100 kHz. The magnitude of the alternative signal is 20 mV.

■ RESULTS AND DISCUSSION

Figure 1 schematically shows the process for synthesizing vertically aligned SnO$_2$ nanotube arrays by using ZnO nanowires as a sacrificial template. The process starts with growing vertically aligned ZnO nanowires on ITO-coated glass substrate by a hydrothermal method. This is followed by conversion of ZnO nanowire arrays to SnO$_2$ nanotubes via SnO$_2$ deposition and simultaneous ZnO dissolution by placing the ZnO nanowire array in an aqueous solution of (NH$_4$)$_2$SnF$_6$ and H$_3$BO$_3$. The conversion process can be described by the following chemical reactions:[18−20]

$$SnF_6^{2-} + 2H_2O \rightarrow SnO_2 + 6F^- + 4H^+ \tag{1}$$

$$H_3BO_3 + 4HF \rightarrow HBF_4 + 3H_2O \tag{2}$$
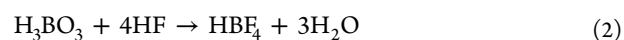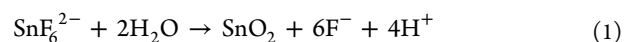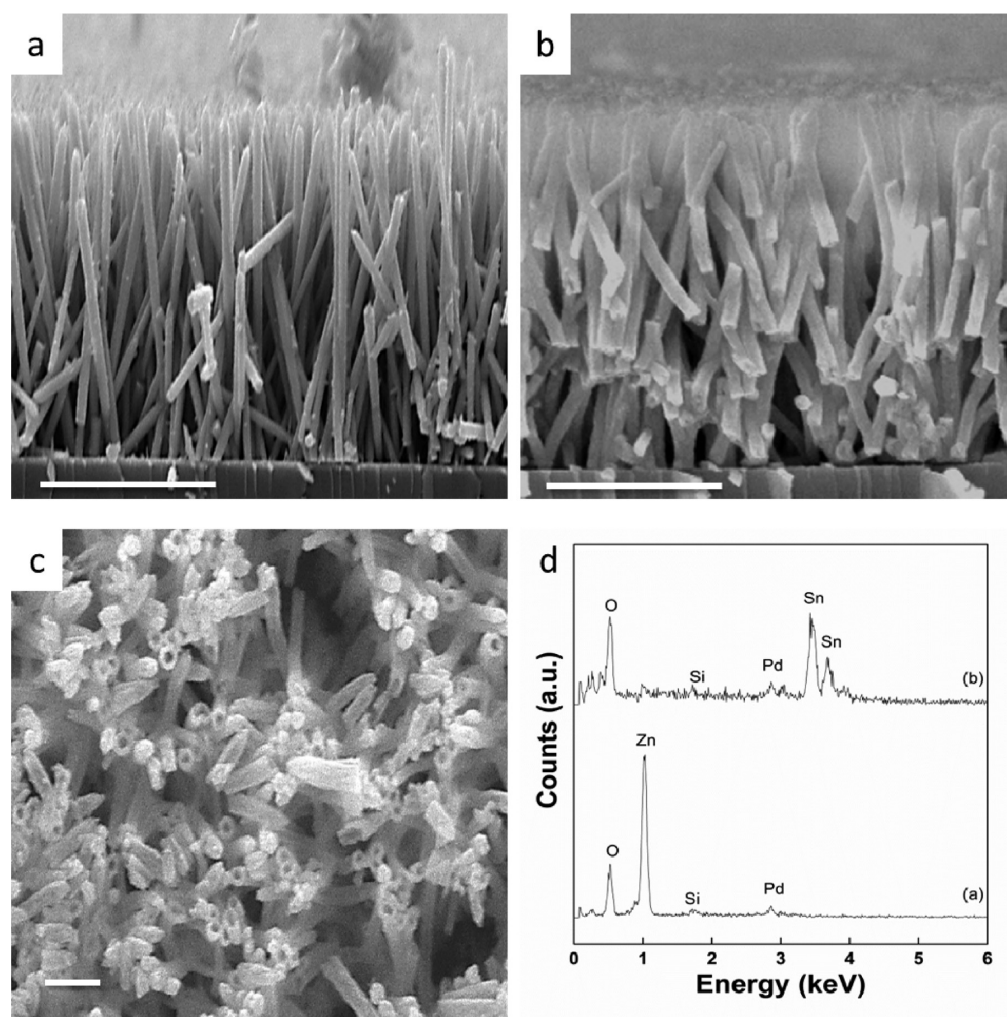
Figure 2. ZnO nanowires and converted SnO$_2$ nanotube arrays. (a) SEM image of a ZnO nanowire array on ITO. Scale bar, 5 μm. (b) SEM image of a converted SnO$_2$ nanotube array. Scale bar, 5 μm. (c) Top-view SEM image of a SnO$_2$ nanotube array. Scale bar, 2 μm. (d) EDX spectra for a ZnO nanowire array, curve a, and a SnO$_2$ nanotube array after conversion, curve b.
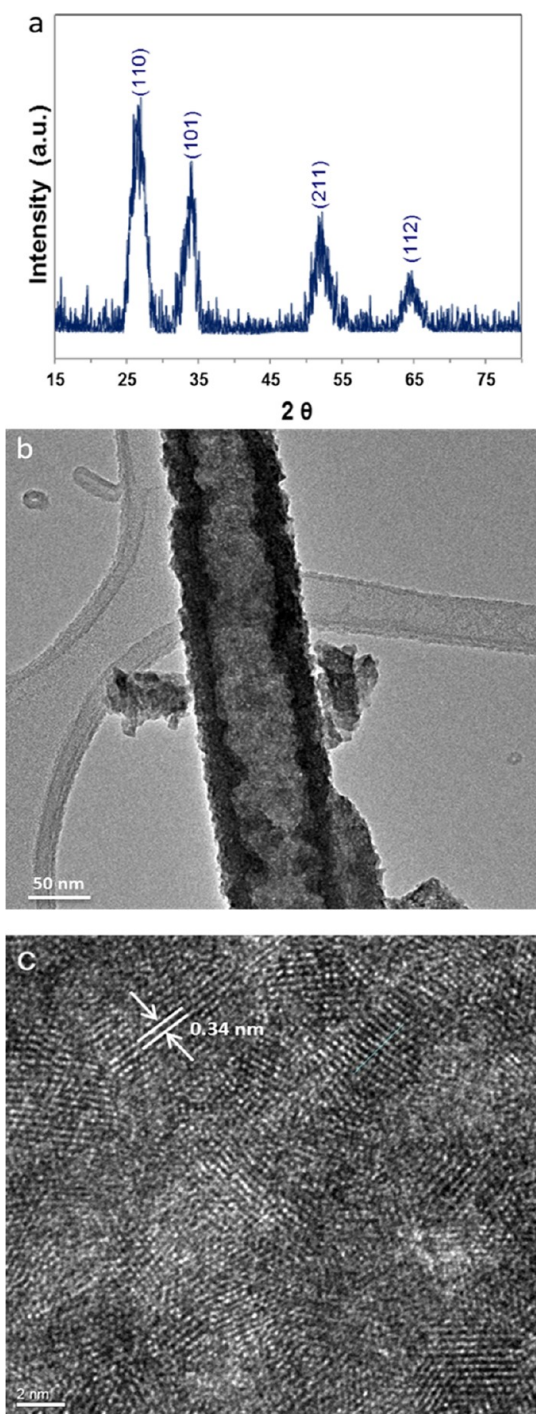
$$ZnO + 2H^+ \rightarrow Zn^{2+} + H_2O \qquad (3)$$
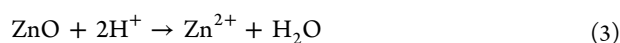
During the conversion process, (NH$_4$)$_2$SnF$_6$ hydrolyses on the surface of the nanowires, resulting in the deposition of SnO$_2$ on the surface of ZnO nanowires. (NH$_4$)$_2$SnF$_6$ hydrolysis also results in formation of acids which aids in the dissolution of ZnO. It should be noted that a small amount of HF may be present in the solution after the conversion process and necessary precautions need to be taken.

Figure 2a shows a representative cross-section scanning electron microscopy (SEM) image of a ZnO nanowire array synthesized by the hydrothermal method previously developed by our group.[17] The wires are 10 μm in length and 150−200 nm in diameter. Parts b and c of Figure 2 show representative cross-section and top-view SEM images of a SnO$_2$ nanotube array. It is observed that the SnO$_2$ nanotubes retain the length of ZnO wires, most of them are open at the top end, and the hollow cores have approximately the same width as the original ZnO wires. Figure 2d shows energy dispersive X-ray (EDX) spectra recorded before (curve a) and after (curve b) the conversion process. In comparison to curve a, curve b shows strong peaks for Sn and O and no detectable peak for Zn, indicating that most of the ZnO nanowires have been converted to SnO$_2$ nanotubes.

Figure 3a shows the X-ray diffraction (XRD) pattern for the SnO$_2$ nanotubes. The XRD pattern can be indexed to tetragonal rutile structured SnO$_2$ (JCPDS card no.: 41-1445). No peaks corresponding to crystalline ZnO were detected, confirming the conversion of ZnO nanowires to SnO$_2$ nanotubes. The as-synthesized SnO$_2$ nanotubes are polycrystalline. The size of individual SnO$_2$ crystals in the polycrystalline nanotubes was estimated by using the Scherrer equation, $D = 0.89\lambda/\beta(\cos\theta)$, where λ is the wavelength of the X-ray (1.54056 Å), β is the peak width at half-maximum in radians, and θ is the Bragg angle.[21,22] Using this equation, the mean particle size was estimated to be 3.3 nm. Figure 3b shows a transmission electron microscopy (TEM) image of an individual SnO$_2$ nanotube, where the hollow core and a wall of 15−20 nm thick can be clearly seen. Figure 3c shows a high-resolution TEM (HRTEM) image of the wall of an individual SnO$_2$ nanotube. The lattice spacing of 0.34 nm shown in Figure 3c corresponds to the (110) plane of SnO$_2$.
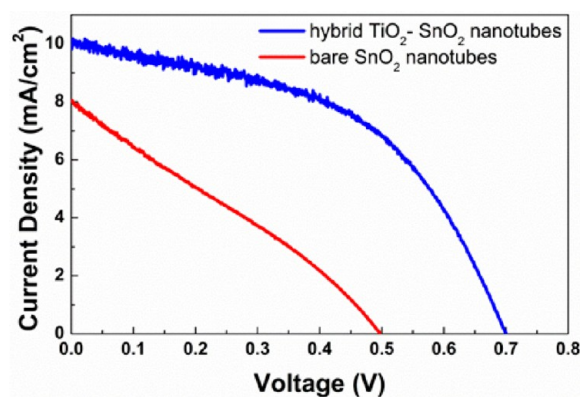
The synthesized SnO$_2$ nanotubes were then used to fabricate DSCs. The red curve in Figure 4 shows the photovoltaic performance of a representative DSC based on SnO$_2$ nanotube arrays. The DSC yielded an efficiency of 1.13% with a short-circuit current (J_{SC}) of 8.05 mA/cm^2 and a V_{OC} of 0.50 V. The V_{OC} obtained is almost 0.20 V higher than those reported for

Figure 4. $I-V$ characteristics of DSCs using SnO_2 nanotube arrays with (blue curve) and without (red curve) TiO_2 coating.

Figure 3. (a) X-ray diffraction pattern for a SnO_2 nanotube array. (b) TEM image for a single SnO_2 nanotube. (c) HRTEM image, showing lattice spacing corresponding to the (110) plane for SnO_2.

SnO_2 nanoparticle based DSCs.[15,16] This increase in V_{OC} could be attributed mainly to the faster electron transport and lower recombination rates for the nanotube based DSC. These factors were verified by studying the recombination kinetics discussed later. The measured J_{SC} was significantly higher than the previously reported J_{SC} for similar DSCs based on SnO_2 1-D nanostructures.[23] This could be mainly attributed to the higher roughness factor, resulting from longer nanotubes of our arrays, compared to previously reported SnO_2 1-D nanostructures. Increase in roughness factor would imply higher dye loading

and consequently higher light harvesting efficiency and higher current densities.

However, V_{OC} and fill factors (ff) for these devices are still low when compared to typical TiO_2-based devices, which is characteristic of SnO_2 as a photoanode.[15,23,24] Efficiency of DSCs based on photoanodes of SnO_2 has been shown to improve by coating the surface of SnO_2 with a conformal barrier layer such as TiO_2 or Al_2O_3.[13,16,24] We here use a liquid-phase deposition method to coat the walls of SnO_2 nanotubes with a thin layer of TiO_2. The method involved immersing a SnO_2 nanotube array in a solution of $(NH_4)_2TiF_6$ and H_3BO_3 for up to 30 min, and the deposition of TiO_2 can be described by the following chemical reactions:[25]

$$TiF_6{}^{2-} + 2H_2O \rightarrow TiO_2 + 6F^- + 4H^+ \tag{4}$$

$$H_3BO_3 + 4HF \rightarrow HBF_4 + 3H_2O \tag{5}$$
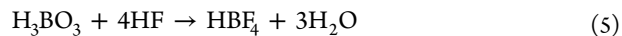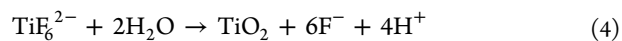
Parts a and b of Figure 5 show an SEM image and an EDX spectrum, respectively, of the SnO_2 nanotube array coated with TiO_2, indicating fairly uniform deposition of TiO_2 while retaining the morphology of the original SnO_2 nanotube array. Parts c and d of Figure 5 show a TEM image and a line-scan EDX profile, respectively, of a single TiO_2-coated SnO_2 nanotube, confirming uniform deposition of a 20−25 nm thick TiO_2 layer on the SnO_2 nanotube.

DSCs were fabricated using these hybrid TiO_2−SnO_2 nanotubes. A representative $I-V$ characteristic of these DSCs was shown by using a blue curve in Figure 4. The photovoltaic performances of DSCs based on (i) SnO_2 nanotubes and (ii) hybrid TiO_2−SnO_2 nanotubes were summarized and compared in Table 1. In comparison, coating the SnO_2 nanotubes with a thin layer of TiO_2 led to a significant improvement in V_{OC} and ff——V_{OC} increased from 0.50 to 0.70 V and ff from 0.28 to 0.50. The much improved photovoltaic performance could be mainly attributed to slower recombination rates due to surface passivation of sub-band-edge surface states.[8] The conduction band-edge of SnO_2 is 0.4 V more positive than TiO_2.[15] Thus, the electrons injected into TiO_2 from the dye would be readily injected into the SnO_2 nanotubes, allowing fast electron transport to the current-collecting surface. TiO_2 forms an energy barrier, forcing electrons to travel toward the current-collecting surface.[13,15] These factors result in considerable reduction in recombination rate, leading to improved V_{OC} and the cell efficiency.

Our best performing cell delivered an efficiency of 3.53%, with J_{SC} of 10.08 mA/cm^2, V_{OC} of 0.70 V, and ff of 0.50. This
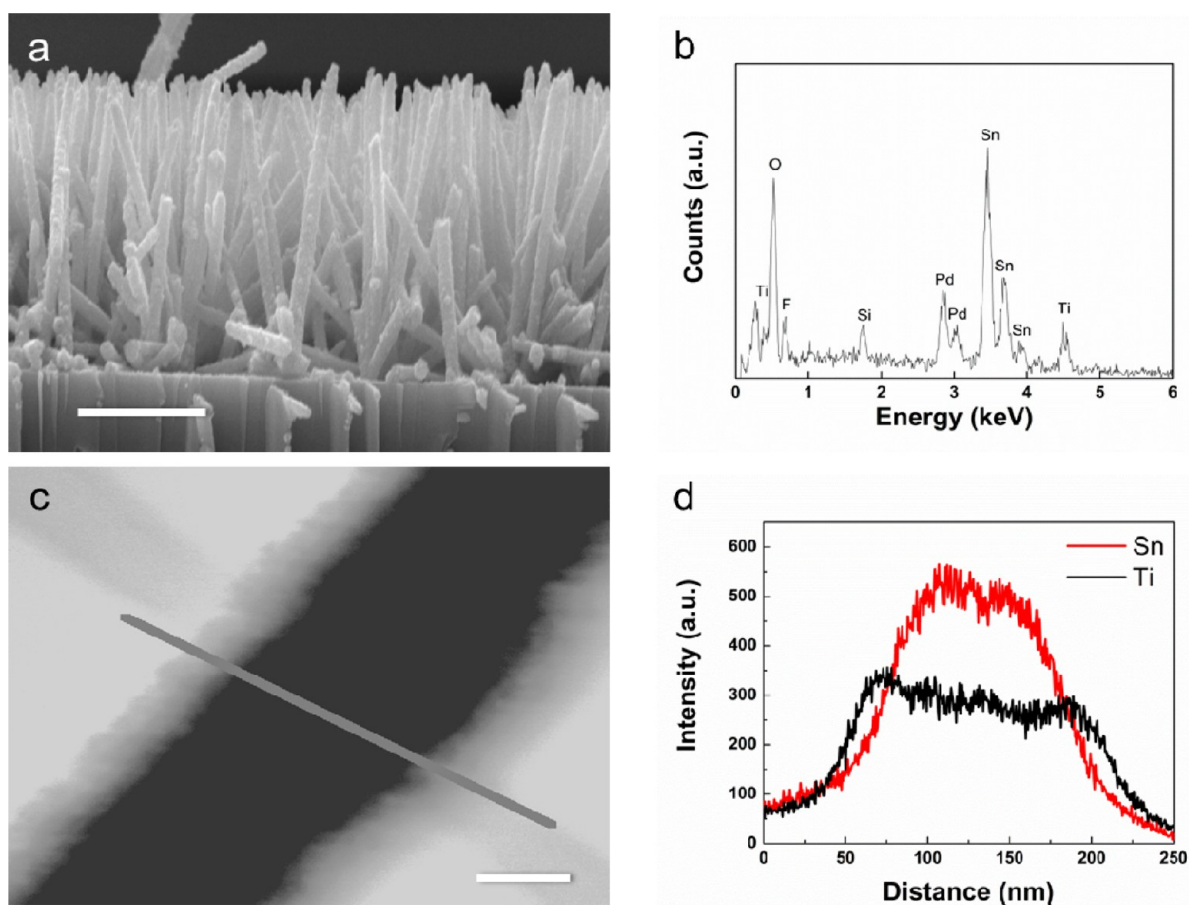
Figure 5. SnO$_2$ nanotubes coated with TiO$_2$. (a) SEM image. Scale bar, 5 μm. (b) EDX spectra. (c) TEM image of a TiO$_2$-coated SnO$_2$ nanotube. Scale bar, 50 nm. (d) Line-scan EDX profile obtained along the line shown in part c.

**Table 1. Photovoltaic Performance Data of DSCs Based on (i) Bare SnO$_2$ Nanotubes and (ii) TiO$_2$-Coated SnO$_2$ Nanotubes**

	bare SnO$_2$ nanotubes	TiO$_2$-coated SnO$_2$ nanotubes
J_{SC} (mA/cm^2)	7.99 ± 0.06	9.91 ± 0.17
V_{OC} (V)	0.49 ± 0.01	0.68 ± 0.02
ff	0.27 ± 0.01	0.49 ± 0.01
η (%)	1.06 ± 0.07	3.47 ± 0.06

efficiency is still low when compared to typical TiO$_2$ nanoparticle-based DSCs. This is mainly due to the low internal surface area of our nanotube arrays when compared to a nanoparticle film. This results in lower dye adsorption and hence lower light absorption. This constraint may be overcome by synthesizing longer nanotubes. Recently, we have reported a method for synthesizing multilayer ZnO nanowire arrays with lengths of up to 40 μm.[25] Work is currently underway to convert these multilayer assemblies into SnO$_2$ nanotubes.
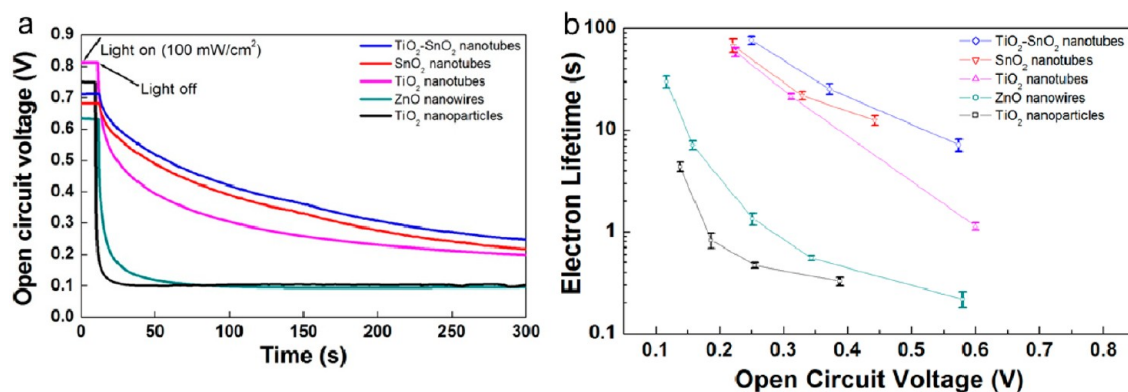
Figure 6. Open-circuit voltage decay curve and calculated electron recombination lifetime for five different anodes: (i) TiO$_2$-coated SnO$_2$ nanotubes, (ii) SnO$_2$ nanotubes, (iii) TiO$_2$ nanotubes, (iv) ZnO nanowires, and (v) TiO$_2$ nanoparticles. (a) Voltage-decay curve. (b) Electron lifetime determined from open-circuit voltage decay measurement.
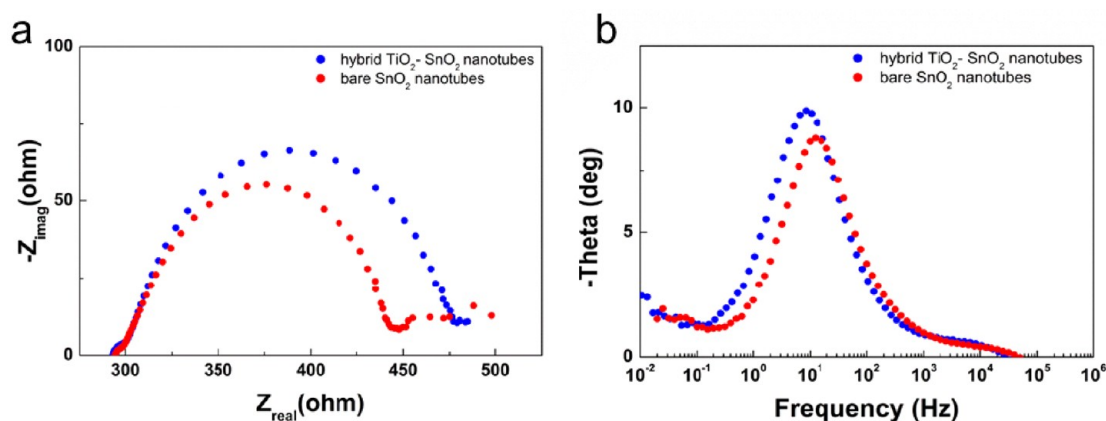
Figure 7. Electrochemical impedance spectroscopy (EIS) for DSCs based on (i) hybrid TiO_2–SnO_2 nanotubes and (ii) bare SnO_2 nanotube arrays under illumination of AM 1.5G simulated sunlight at an applied bias of V_{OC}. (a) Nyquist plots. (b) Bode phase angle versus frequency plots.

To further understand the performance of DSCs based on SnO_2 nanotubes and hybrid TiO_2–SnO_2 nanotubes, transient photovoltage measurements were conducted, by monitoring the V_{OC} as a function of time upon turning off the illumination, to study the electron recombination kinetics. The experiments were repeated with DSCs based on TiO_2 nanoparticles, TiO_2 nanotubes, and ZnO nanowires of the same thickness, and the results were compared. Figure 6a shows V_{OC} decay as a function of time for five different anodes: (i) TiO_2-coated SnO_2 nanotubes, (ii) SnO_2 nanotubes, (iii) TiO_2 nanotubes, (iv) ZnO nanowires, and (v) TiO_2 nanoparticles. It was observed that DSCs based on TiO_2-coated SnO_2 nanotubes and SnO_2 nanotubes showed a much slower V_{OC} decay rate than DSCs based on the other three electrodes, indicating much slower recombination rates. From the V_{OC} decay rate, the photoelectron recombination lifetime (τ_r) may be determined by the following equation:[26,27]

$$\tau_r = -\left(\frac{k_B T}{e}\right) \times \left(\frac{dV_{OC}}{dt}\right)^{-1}$$

(6)

where k_B is the Boltzmann constant and T is temperature. The calculated τ_r is plotted in Figure 6b for five different electrodes. It is observed that the τ_r values for TiO_2–SnO_2 nanotubes, SnO_2 nanotubes, and TiO_2 nanotubes are almost 2 orders of magnitude higher than that for TiO_2 nanoparticles. They are also much higher than the literature reported τ_r for SnO_2 nanoparticles.[15]

The much larger τ_r in the nanotubes compared to nanoparticle films may be explained by an internal radial electric field that is developed within the walls of the nanotubes. This electric field drives the electrons away from the interface, preventing recombination with the electrolyte.[18] The primary reason for longer lifetimes in TiO_2 based nanotubes as compared to ZnO nanowires is due to the intrinsic material properties. It has been reported that the conduction band of TiO_2 is composed of d-orbital electrons that are less susceptible to recombination than the electrons in ZnO.[28] Among the five different electrodes, the hybrid TiO_2–SnO_2 electrode exhibits the slowest recombination rates, slightly slower than the bare SnO_2 nanotube arrays. This could be due to the energy barrier formed by the TiO_2 coating, forcing the electrons to flow toward the current collecting surface and preventing the electrons from flowing in the opposite direction. Introduction of TiO_2 may have also passivated the reactive low-energy SnO_2

surface states.[8] These factors lead to further lowering of the recombination rates, resulting in enhanced V_{OC} and ff for DSCs based on the hybrid TiO_2–SnO_2 electrodes.

We also performed electrochemical impedance spectroscopy (EIS) to further understand the improved performance of the hybrid electrodes. Figure 7a shows Nyquist plots for DSCs based on hybrid TiO_2–SnO_2 and bare SnO_2 nanotubes obtained by EIS carried out under illumination of AM 1.5G simulated sunlight at an applied bias of V_{OC}. The impedance components of the interfaces in the DSCs are observed in three different frequency regimes. The arcs observed in the EIS spectra may be assigned to the impedances due to the conducting layer/semiconductor interface, Pt/electrolyte interface, and photoanode/dye/electrolyte interface.[29,30] In the middle frequency range of 0.1–10^4 Hz, the semicircle on the Nyquist plot is associated with the charge transfer across the photoanode/dye/electrolyte interface and the size of the semicircle represents the resistance to recombination.

As can be seen from the Nyquist plots in Figure 7a, the semicircle observed in the middle frequency range is larger in the case of the hybrid TiO_2–SnO_2 nanotube photoanode than that for the bare SnO_2 nanotube photoanode. This indicates increased recombination resistance, which results in lower recombination rates at the photoanode/dye/electrolyte interface for DSCs using the hybrid TiO_2–SnO_2 photoanodes. The electron lifetime, τ_r, can be estimated from the maximum angular frequency of the impedance semicircle arc at middle frequencies, according to the relation:

$$\tau_r = \frac{1}{2\pi f_{max}}$$

(7)

where f_{max} is the maximum frequency of the midfrequency peak.[24] Thus, a peak shift to a lower frequency represents longer electron recombination lifetime. For DSCs with a hybrid TiO_2–SnO_2 photoanode, a longer electron lifetime of 18.9 ms is obtained compared to 12.8 ms for DSCs based on a bare SnO_2 photoanode. The longer electron recombination lifetime of the hybrid TiO_2–SnO_2 photoanode compared to the bare SnO_2 photoanode is in agreement with the trend observed in the transient photovoltage measurement. It needs to be noted that the absolute values for recombination lifetimes obtained by EIS differ from those reported by photovoltage decay measurements. The primary reason for this could be that, in photovoltage decay measurements, the cell was allowed to

Table 2. Parameters Determined by EIS for Photoanodes Based on (i) Bare SnO₂ Nanotubes and (ii) TiO₂-Coated SnO₂ Nanotubes

	R_w (Ω)	R_k/R_w	k_{eff} (s^{-1})	τ_r (ms)	D_{eff} ($\times 10^4$ cm^2/s)	L_n (μm)
bare SnO₂ nanotubes	145 ± 15	12.75 ± 1.45	11.9 ± 1.08	12.89 ± 1.17	1.71 ± 0.33	14.72 ± 0.79
TiO₂-coated SnO₂ nanotubes	165 ± 20	33.45 ± 2.35	8.39 ± 0.06	18.91 ± 0.14	2.89 ± 0.11	23.31 ± 0.12

decay through low carrier density states, resulting in longer electron lifetimes. On the other hand, EIS measurements were performed at open-circuit voltage, when electron density is the highest.

Electrons with longer τ_r can obtain longer diffusion length (L_n) and more easily escape the electron recombination. L_n can be derived using the following equations:[31−33]

$$L_n^2 = D_{eff} \times \tau_r \tag{8}$$

$$D_{eff} = (R_k/R_w)L^2 k_{eff} \tag{9}$$

where R_w, R_k, L, D_{eff}, and k_{eff} represent the resistance of electron transport in photoanode, resistance of charge transfer related to recombination, thickness of the photoanode, effective electron diffusion coefficient, and constant of effective rate for recombination, respectively. The values of these parameters were estimated from the central arc of Nyquist and Bode phase plots as described by J. L. Song.[33] R_w is determined from the diameter of the middle semicircle in the Nyquist plot shown in Figure 7a, and R_k is determined from the diameter of the middle semicircle in the Nyquist plot obtained under dark conditions (Figure S1, Supporting Information). k_{eff} is estimated from the maximum peak frequency obtained from the Bode phase plot in Figure 7b. The calculated values are tabulated in Table 2. The results indicate that the hybrid photoanode is superior to the bare SnO₂ nanotube photoanode with significantly larger L_n, D_{eff}, and τ_r but smaller k_{eff}. Besides the expected increase in electron lifetime, a larger effective diffusion coefficient was also observed in the case of the hybrid photoanode. The reason for large D_{eff} could be due to the passivation of the low energy SnO₂ surface trap states. These results explain the improved photovoltaic performance of the hybrid TiO₂−SnO₂ photoanode as compared to the bare SnO₂ photoanode.

CONCLUSIONS

We have developed feasible processes to synthesize long, vertically ordered SnO₂ and hybrid TiO₂−SnO₂ nanotube arrays. All the processes involved in the synthesis are carried out in aqueous solution at low temperatures. We have fabricated DSCs by using the vertically ordered nanotube arrays of both SnO₂ and hybrid TiO₂−SnO₂, and found that coating the SnO₂ nanotubes with a thin layer of TiO₂ significantly improves the DSC performance. The best performing cell is fabricated by using the hybrid TiO₂−SnO₂ anodes, which yields an efficiency of 3.53%. In addition, we have studied the photogenerated electron recombination kinetics of different photoanode materials and observed that the electron recombination lifetime in the anodes of SnO₂ and hybrid TiO₂−SnO₂ nanotubes is significantly higher than that in nanoparticle-based anodes and also significantly higher than 1-D nanostructures of ZnO and TiO₂. This result opens up the possibility of using redox mediators with faster kinetics, which would otherwise be hampered by fast recombination of electrons. The use of vertically ordered 1-D nanostructures as anodes in DSCs may also facilitate filling of the pores with solid

hole transporting materials, making them promising candidate anodes for solid-state DSCs.[10,11] Furthermore, the vertically ordered SnO₂ nanostructures may find other applications in gas sensors[34] and lithium-ion batteries.[35,36]

ASSOCIATED CONTENT

Ⓢ Supporting Information
Table enlisting the photovoltaic parameters for different electrodes used for open-circuit transient photovoltage decay studies; electrochemical impedance spectroscopy (EIS) spectra for DSCs based on hybrid TiO₂−SnO₂ nanotubes and bare SnO₂ nanotube arrays under dark conditions. This material is available free of charge via the Internet at http://pubs.acs.org.

AUTHOR INFORMATION

Corresponding Author
*E-mail: gaod@pitt.edu.

Notes
The authors declare no competing financial interest.

REFERENCES

(1) Nazeeruddin, M. K.; Kay, A.; Rodicio, I.; Humphrey-Baker, R.; Müller, E.; Liska, P.; Vlachopoulos, N.; Grätzel, M. Conversion of Light to Electricity by Cis-X2bis(2,2′-Bipyridyl-4,4′-Dicarboxylate)-Ruthenium(II) Charge-Transfer Sensitizers (X = Cl-, Br-, I-, CN-, And SCN-) on Nanocrystalline Titanium Dioxide Electrodes. *J. Am. Chem. Soc.* **1993**, *115*, 6382−6390.

(2) Hardin, B. E.; Snaith, H. J.; McGehee, M. D. The Rennaisance of Dye-Sensitized Solar Cells. *Nat. Photonics* **2012**, *6*, 162−169.

(3) Yella, A.; Lee, H.-W.; Tsao, H. N.; Yi, C.; Chandiran, A. K.; Nazeeruddin, M. K.; Diau, E. W.-G.; Yeh, C.-Y.; Zakeeruddin, S. M.; Grätzel, M. Porphyrin-Sensitized Solar Cells with Cobalt (II/III)-Based Redox Electrolyte Exceed 12% Efficiency. *Science* **2011**, *334*, 629−634.

(4) Hendry, E.; Koeberg, M.; O'Regan, B.; Bonn, M. Local Field Effects on Electron Transport in Nanostructured TiO₂ Revealed by Terahertz Spectroscopy. *Nano Lett.* **2006**, *6*, 755−759.

(5) Law, M.; Greene, L. E.; Johnson, J. C.; Saykally, R.; Yang, P. Nanowire Dye-Sensitized Solar Cells. *Nat. Mater.* **2005**, *4*, 455−459.

(6) Chappel, S.; Zaban, A. Nanoporous SnO₂ Electrodes for Dye-Sensitized Solar Cells: Improved Cell Performance by the Synthesis of 18 nm SnO₂ Colloids. *Sol. Energy Mater. Sol. Cells* **2002**, *71*, 141−152.

(7) Sayama, K.; Sugihara, H.; Arakawa, H. Photoelectrochemical Properties of a Porous Nb₂O₅ Electrode Sensitized by a Ruthenium Dye. *Chem. Mater.* **1998**, *10*, 3825−3832.

(8) Ramasamy, E.; Lee, J. Ordered Mesoporous SnO₂-Based Photoanodes for High-Performance Dye-Sensitized Solar Cells. *J. Phys. Chem. C* **2010**, *114*, 22032−22037.

(9) Seager, C. H.; Myers, S. M. Quantitative Comparisons of Dissolved Hydrogen Density and the Electrical and Optical Properties of ZnO. *J. Appl. Phys.* **2003**, *94*, 2888−2894.

(10) Gubbala, S.; Chakrapani, V.; Kumar, V.; Sunkara, M. K. Band-Edge Engineered Hybrid Structures for Dye-Sensitized Solar Cells Based on SnO₂ Nanowires. *Adv. Funct. Mater.* **2008**, *18*, 2411−2418.

3238

dx.doi.org/10.1021/jp3096727 | *J. Phys. Chem. C* 2013, 117, 3232−3239

(11) Martinson, A. B. F.; Hamann, T. W.; Pellin, M. J.; Hupp, J. T. New Architectures for Dye-Sensitized Solar Cells. *Chem.—Eur. J.* **2008**, *14*, 4458−4467.

(12) Green, A. N. M.; Palomares, E.; Haque, S. A.; Kroon, J. M.; Durrant, J. R. Charge Transport versus Recombination in Dye-Sensitized Solar Cells Employing Nanocrystalline TiO₂ and SnO₂ Films. *J. Phys. Chem. B* **2005**, *109*, 12525−12533.

(13) Benkö, G.; Myllyperkiö, P.; Pan, J.; Yartsev, A. P.; Sundström, V. Photoinduced Electron Injection from Ru(dcbpy)₂(NCS)₂ to SnO₂ and TiO₂ Nanocrystalline Films. *J. Am. Chem. Soc.* **2003**, *125*, 1118−1119.

(14) Kay, A.; Grätzel, M. Dye-Sensitized Core−Shell Nanocrystals: Improved Efficiency of Mesoporous Tin Oxide Electrodes Coated with a Thin Layer of an Insulating Oxide. *Chem. Mater.* **2002**, *14*, 2930−2935.

(15) Tiwana, P.; Docampo, P.; Johnston, M. B.; Snaith, H. J.; Herz, L. M. Electron Mobility and Injection Dynamics in Mesoporous ZnO, SnO₂, and TiO₂ Films Used in Dye-Sensitized Solar Cells. *ACS Nano* **2011**, *5*, 5158−5166.

(16) Chappel, S.; Chen, S.-G.; Zaban, A. TiO₂-Coated Nanoporous SnO₂ Electrodes for Dye-Sensitized Solar Cells. *Langmuir* **2002**, *18*, 3336−3342.

(17) Xu, C.; Shin, P.; Cao, L.; Gao, D. Preferential Growth of Long ZnO Nanowire Array and Its Application in Dye-Sensitized Solar Cells. *J. Phys. Chem. C* **2010**, *114*, 125−129.

(18) Xu, C.; Shin, P. H.; Cao, L.; Wu, J.; Gao, D. Ordered TiO₂ Nanotube Arrays on Transparent Conductive Oxide for Dye-Sensitized Solar Cells. *Chem. Mater.* **2010**, *22*, 143−148.

(19) Lee, J.-H.; Leu, I.-C.; Hsu, M.-C.; Chung, Y.-W.; Hon, M.-H. Fabrication of Aligned TiO₂ One-Dimensional Nanostructured Arrays Using a One-Step Templating Solution Approach. *J. Phys. Chem. B* **2005**, *109*, 13056−13059.

(20) Deki, S.; Iizuka, S.; Horie, A.; Mizuhata, M.; Kajinami, A. Liquid-Phase Infiltration (LPI) Process for the Fabrication of Highly Nano-Ordered Materials. *Chem. Mater.* **2004**, *16*, 1747−1750.

(21) Birks, L. S.; Friedman, H. Particle Size Determination from X-ray Line Broadening. *J. Appl. Phys.* **1946**, *17*, 687−692.

(22) Ishikawa, K.; Yoshikawa, K.; Okada, N. Size Effect on the Ferroelectric Phase Transition in PbTiO₃ Ultrafine Particles. *Phys. Rev. B* **1988**, *37*, 5852−5855.

(23) Wang, Y.; Guo, M.; Zhang, M.; Wang, X. Hydrothermal Preparation and Photoelectrochemical Performance of Size-Controlled SnO₂ Nanorod Arrays. *CrystEngComm* **2010**, *12*, 4024−4027.

(24) Qian, J.; Liu, P.; Xiao, Y.; Jiang, Y.; Cao, Y.; Ai, X.; Yang, H. TiO₂-Coated Multilayered SnO₂ Hollow Microspheres for Dye-Sensitized Solar Cells. *Adv. Mater.* **2009**, *21*, 3663−3667.

(25) Xu, C.; Wu, J.; Desai, U. V.; Gao, D. Multilayer Assembly of Nanowire Arrays for Dye-Sensitized Solar Cells. *J. Am. Chem. Soc.* **2011**, *133*, 8122−8125.

(26) Bisquert, J.; Zaban, A.; Greenshtein, M.; Mora-Seró, I. Determination of Rate Constants for Charge Transfer and the Distribution of Semiconductor and Electrolyte Electronic Energy Levels in Dye-Sensitized Solar Cells by Open-Circuit Photovoltage Decay Method. *J. Am. Chem. Soc.* **2004**, *126*, 13550−13559.

(27) Zaban, A.; Greenshtein, M.; Bisquert, J. Determination of the Electron Lifetime in Nanocrystalline Dye Solar Cells by Open-Circuit Voltage Decay Measurements. *ChemPhysChem* **2003**, *4*, 859−864.

(28) Bandaranayake, K. M. P.; Indika Senevirathna, M. K.; Prasad Weligamuwa, P. M. G. M.; Tennakone, K. Dye-Sensitized Solar Cells Made from Nanocrystalline TiO₂ Films Coated with Outer Layers of Different Oxide Materials. *Coord. Chem. Rev.* **2004**, *248*, 1277−1281.

(29) Lee, S.; Cho, I.-S.; Lee, J. H.; Kim, D. H.; Kim, D. W.; Kim, J. Y.; Shin, H.; Lee, J.-K.; Jung, H. S.; Park, N.-G.; et al. Two-Step Sol−Gel Method-Based TiO₂ Nanoparticles with Uniform Morphology and Size for Efficient Photo-Energy Conversion Devices. *Chem. Mater.* **2010**, *22*, 1958−1965.

(30) Wang, Q.; Moser, J.-E.; Grätzel, M. Electrochemical Impedance Spectroscopic Analysis of Dye-Sensitized Solar Cells. *J. Phys. Chem. B* **2005**, *109*, 14945−14953.

(31) Choi, H.; Kang, S. O.; Ko, J.; Gao, G.; Kang, H. S.; Kang, M.-S.; Nazeeruddin, M. K.; Grätzel, M. An Efficient Dye-Sensitized Solar Cell with an Organic Sensitizer Encapsulated in a Cyclodextrin Cavity. *Angew. Chem., Int. Ed.* **2009**, *48*, 5938−5941.

(32) Adachi, M.; Sakamoto, M.; Jiu, J.; Ogata, Y.; Isoda, S. Determination of Parameters of Electron Transport in Dye-Sensitized Solar Cells Using Electrochemical Impedance Spectroscopy. *J. Phys. Chem. B* **2006**, *110*, 13872−13880.

(33) Song, J.; Yin, Z.; Yang, Z.; Amaladass, P.; Wu, S.; Ye, J.; Zhao, Y.; Deng, W.-Q.; Zhang, H.; Liu, X.-W. Enhancement of Photgenerated Electron Transport in Dye-Sensitized Solar Cells with Introduction of a Reduced Graphene Oxide-TiO₂ Junction. *Chem.—Eur. J.* **2011**, *17*, 10832−10837.

(34) Xi, G.; Ye, J. Ultrathin SnO₂ Nanorods: Template- and Surfactant-Free Soultion Phase Synthesis, Growth Mechanism, Optical, Gas-Sensing, and Surface Adsorption Properties. *Inorg. Chem.* **2010**, *49*, 2302−2309.

(35) Kim, D.-W.; Hwang, I.-S.; Kwon, S. J.; Kang, H.-Y.; Park, K.-S.; Choi, Y.-J.; Choi, K.-J.; Park, J.-G. Highly Conductive Coaxial SnO₂-In₂O₃ Heterostructured Nanowires for Li Ion Battery Electrodes. *Nano Lett.* **2007**, *7*, 3041−3045.

(36) Park, M.-S.; Wang, G.-X.; Kang, Y.-M.; Wexler, D.; Dou, S.-X.; Liu, H.-K. Preparation and Electrochemical Properties of SnO₂ Nanowires for Application in Lithium-Ion Batteries. *Angew. Chem., Int. Ed.* **2007**, *46*, 750−753.